Rate Constants for D + C_2H_2 → C_2HD + H at High Temperature: Implications to the High Pressure Rate Constant for H + C_2H_2 → C_2H_3†

J. V. Michael,* M.-C. Su,‡ J. W. Sutherland,§ L. B. Harding, and A. F. Wagner

Chemistry Division, Argonne National Laboratory, Argonne, Illinois 60439

Received: April 30, 2003; In Final Form: July 10, 2003

The reflected shock tube technique with D atom atomic resonance absorption spectrometry (ARAS) detection has been used to study the bimolecular reaction, D + C_2H_2 → C_2HD + H. D atoms were produced from the thermal decomposition of C_2D_5I above ∼1150 K. The initially formed C_2D_5 radicals rapidly decompose to give D + C_2D_4. Rate constant values were obtained from both reactant and product hydrogen atom measurements, and these were found to be identical within experimental error. The title reaction proceeds through a vibrationally excited vinyl radical, and the equivalence of results based on reactant and product measurements suggests that radical stabilization is negligible over the temperature and pressure ranges of the experiments. For 1100 ≤ T ≤ 1630 K, the results can be described by the linear-least-squares Arrhenius expression: $k = (2.77 \pm 0.45) \times 10^{-10} \exp(-3051 \pm 210\ \mathrm{K/T})$ in units of cm^3 $molecule^{-1}$ s^{-1}, with the one standard deviation of the values from the equation being ±10.7%. Application of RRKM theory with negligible stabilization shows that $k = k_{D\infty}\langle k_{f\epsilon}/(k_{f\epsilon} + k_{b\epsilon})\rangle$ where the $k_{i\epsilon}$'s refer to RRKM evaluated specific rate constants for forward and backward dissociations, and $k_{D\infty}$ is the high-pressure limiting rate constant for D addition to acetylene. Hence, the present measurements coupled with earlier measurements and modern ab initio potential energy determinations allow for specification of the high-pressure limiting rate constants. The same model can then be used for the protonated reaction, H + C_2H_2, where a considerable ambiguity has existed for about 30 years.

Introduction

The H + C_2H_2 reaction has been the subject of numerous investigations for over 50 years. Le Roy and co-workers[1] studied this reaction in a low-pressure flow reactor, and this was one of the first reactions ever seriously studied by this technique. In a series of studies performed in the 1960s,[2] the reaction was found to be first-order, in both H atoms and acetylene, and pressure and temperature dependent. No reaction products could be identified suggesting that acetylene simply catalyzes the recombination of H atoms. Subsequently, new and more thorough studies have appeared,[3−9] confirming that this is a classic chemical activation case with the reaction mechanism being

$$H + C_2H_2 \rightarrow C_2H_3^* \quad (1)$$

$$C_2H_3^* \rightarrow C_2H_2 + H \quad (-1)$$

$$C_2H_3^* + M \rightarrow C_2H_3 + M \quad (2)$$

where the asterisk designates vibrational excitation. Hence, the rate constant based on H-atom depletion at any pressure or temperature can be expressed in an RRKM formulation as

$$k_b = k_{1\infty}\int_{\epsilon_0}^{\infty}(\beta\omega/(k_{b\epsilon} + \beta\omega))f(\epsilon)\,d\epsilon \quad (3)$$

where $k_{1\infty}$, $k_{b\epsilon}$, β, ω, and $f(\epsilon)$ refer to (a) the high-pressure rate constant for reaction 1, (b) the specific RRKM rate constant for backward dissociation of $C_2H_3^*$, reaction (−1), to give reactants at the threshold energy, ϵ_0, (c) the collisional deactivation efficiency, (d) the collision rate constant, and (e) the normalized chemical activation distribution function originating at ϵ_0 for a given temperature, respectively. In three separate decades, RRKM calculations have been applied[5,6,8,9] with increasing sophistication in order to explain the data that existed at the various times.

In the earliest theoretical work, the primary source for high-pressure rate constants, $k_{1\infty}$, were from Payne and Stief,[4] whose measured values followed the Arrhenius expression, $k_{1\infty} = 9.20 \times 10^{-12} \exp(-1213\ \mathrm{K/T})$ cm^3 $molecule^{-1}$ s^{-1}, over the temperature range, 193−400 K. This suggested an activation energy for reaction 1 of 2.4 kcal mol^{-1}. Empirical electronic structure models[5] and ab initio models[8] were identified, and RRKM calculations were carried out with the constraint that the barrier for reaction 1 should be scaled to the Payne and Stief value of 2.4 kcal mol^{-1}. Though the descriptions of the rate behavior were satisfactory, the implications of the models were inconsistent with the A-factor for the measured high-pressure limit. A transmission coefficient of ∼0.05 was required which subsequently suggested that the reaction was non-RRKM. The problem was potentially understood with the work of Sato and co-workers[6] and Knyazev and Slagle,[9] who both included quantum mechanical tunneling. The latter group made new measurements on vinyl dissociation and also carried out more modern ab initio calculations. However, scaling of the barrier height to 4.0 kcal mol^{-1} was still required. The inclusion of

† Part of the special issue "Charles S. Parmenter Festschrift".

* To whom correspondence should be addressed. Dr. J. V. Michael D-193, Bldg. 200 Argonne National Laboratory Argonne, IL 60439. Phone: (630) 252-3171. Fax: (630) 252-4470. E-mail: Michael@anlchm.chm.anl.gov.

‡ Faculty Research Participant, Department of Educational Programs, Argonne. Permanent address: Department of Chemistry, Butler University, Indianapolis, IN 46208.

§ Present address: Guest Scientist, Energy Sciences and Technology Department, Brookhaven National Laboratory, Upton, NY 11973.

10.1021/jp035170n CCC: $25.00
Published on Web 09/27/2003

quantum mechanical tunneling was a new innovation in the description of this reaction. Including both tunneling and also weak collision effects, Knyazev and Slagle's RRKM calculations then gave an adequate description of all existing data for H + C_2H_2, suggesting that the Payne and Stief results,[4] for the two highest temperatures, were not at the high-pressure limit. Another implication of this work is that, if tunneling is important, then the T-dependence of $k_{1\infty}$ should follow non-Arrhenius behavior, giving the true value for the activation energy only at high temperatures where tunneling factors are near unity. This possibility supplies the motivation for the present high temperature study on the D + C_2H_2 reaction.

Application of RRKM theory for D + C_2H_2 gives the rate constant expression for D-atom depletion as

$$k_{bD} = k_{1D\infty}\int_{\epsilon_0}^{\infty}((k_{f\epsilon} + \beta\omega)/(k_{f\epsilon} + k_{b\epsilon} + \beta\omega))f(\epsilon)\,d\epsilon \quad (4)$$

where all terms are the same as in eq 3; however, in this case, $k_{f\epsilon}$ is the specific RRKM rate constant for forward dissociation from $C_2H_2D^*$ to give C_2HD + H. In this study, the pressure is relatively low and the temperature is high suggesting that stabilization might not favorably compete with both forward and back dissociations. The rate constant would then be, $k_{bD} = k_{1D\infty}\langle k_{f\epsilon}/(k_{f\epsilon} + k_{b\epsilon})\rangle$, where the average is taken over the distribution function, $f(\epsilon)$, and this then becomes the rate constant for the title reaction.

In the present study, rate constants were measured using the thermal dissociation of C_2D_5I as the source of D atoms.[10] As pointed out earlier,[10] this method gives a clean source of D atoms from C_2D_5 radical dissociation formed after the initial C-I bond has been broken; i.e., the overall process is $C_2D_5I = C_2D_4$ + D + I. Both D-depletion and H-formation experiments were performed, and the experiments were carried out with a large excess of C_2H_2 so that the decay of D atoms and the formation of H atoms would be approximately pseudo-first-order.

Experimental Section

The present experiments were performed with the shock tube technique using atomic resonance absorption spectrometric (ARAS) detection. The method and the apparatus currently being used have been previously described.[11,12] Therefore, only a brief description of the experiment will be presented here.

The apparatus consists of a 7 m (4 in. o.d.) 304 stainless steel tube separated from the He driver chamber by a 4-mil unscored 1100-H18 aluminum diaphragm. The tube was routinely pumped between experiments to $<10^{-8}$ Torr by an Edwards Vacuum Products model CR100P packaged pumping system. The velocity of the shock wave was measured with eight equally spaced pressure transducers (PCB Piezotronics, Inc., model 113A21) mounted along the end portion of the shock tube, and temperature and density in the reflected shock wave regime were calculated from this velocity and include corrections for boundary layer perturbations.[13−15] The 4094C Nicolet digital oscilloscope was triggered by delayed pulses that derive from the last velocity gauge signal.

D and H atom atomic resonance absorption spectrometric (ARAS) detection was used to follow $[D]_t$ and $[H]_t$ quantitatively as described previously.[16−18] Adding small amounts of D_2 to the resonance lamp gave measurable Lyman-αD. Because the separation between H- and D-Lyman-α lines is substantial,[18] the D line was isolated by using an H atom atomic filter (a slowly flowing H_2 discharge flow system) between the resonance lamp and the shock tube window in the kinetics experiments.[19] This was necessary because Lyman-αH is still present in the unfiltered lamp. The entire photometer system was radially located at the distance of 6 cm from the endplate. MgF_2 components were used in the photometer optics, and the resonance lamp beam was detected by an EMR G14 solar blind photomultiplier tube.

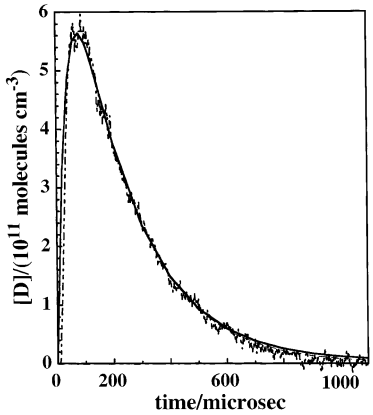

Figure 1. D-atom profile ($[D]_t$ against time) for an experiment with P_1 = 10.97 Torr and M_s = 2.243. T_5 = 1282 K, $\rho_5 = 1.852 \times 10^{18}$ molecules cm^{-3}, $[C_2H_2]_0 = 1.926 \times 10^{14}$ molecules cm^{-3}, and $[C_2D_5I]_0 = 1.49 \times 10^{12}$ molecules cm^{-3}. The line is a simulation with a 41 step mechanism (from ref 10 and including the title reaction), and the fitted second order value for k_{bD} is 2.53×10^{-11} cm^3 molecule^{-1} s^{-1}.

Gases. High purity He (99.995%), used as the driver gas, was from AGA Gases. Scientific grade Kr (99.999%), the diluent gas in reactant mixtures, was from Spectra Gases, Inc. The ∼10 ppm impurities (N_2, 2 ppm; O_2, 0.5 ppm; Ar, 2 ppm; CO_2, 0.5 ppm; H_2, 0.5 ppm; CH_4, 0.5 ppm; H_2O, 0.5 ppm; Xe, 5 ppm; and CF_4, 0.5 ppm) are all either inert or in sufficiently low concentration so as to not perturb H or D atom profiles. Ultrahigh purity grade He (99.999%) for the resonance lamp and high purity H_2 (99.995%) for the atomic filter were from AGA Gases. Research Grade D_2 (99.99%) from Air Products and Chemicals, Inc. was used in the resonance lamp. Analytical grade C_2D_5I (99%) from Aldrich Chemical Co., Inc., was purified by bulb-to-bulb distillation, retaining only the middle third. C_2H_2 was obtained from AGA Gases and was also subjected to bulb-to-bulb distillation, retaining the middle third. Test gas mixtures were accurately prepared from pressure measurements using a Baratron capacitance manometer and were stored in an all glass vacuum line.

Results

D-atom decay and H-atom build-up were observed in separate experiments, and Figures 1 and 2 show typical examples for both types of experiments. To establish whether first-order analysis would be sufficient, we used a mechanism from a previous study[10] on the D + CH_3 reaction to simulate profiles, with additional reactions added, including the title reaction. The solid line in Figure 1 is such a simulation. The dashed line is a simulation that includes only the title reaction and the thermal decomposition of C_2D_5I. $[C_2D_5I]_t$ is negligible after ∼150−200 μs in which case D atom depletion then should be strictly first-order; that is, a plot of $\ln[D]_t$ against time should be linear with the first-order decay constant, $k_{first} = k_{bD}[C_2H_2]$. The small long time difference between the two simulations in Figure 1 arises from the secondary reaction, H + $C_2D_4 \rightarrow$ D + C_2HD_3 which occurs to a minor extent due to the formation of C_2D_4 from C_2D_5 radical dissociation. However, a first-order analysis applied to both simulations gives values for k_{bD} that differ by <5% from that obtained using first-order analysis of the experiment, an example of which is shown in Figure 3 for the experiment in Figure 1. Conditions and k_{bD} values for all D

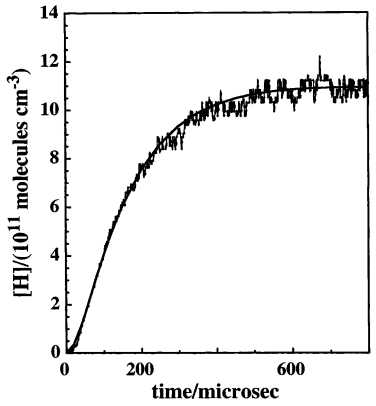

Figure 2. H-atom profile ($[H]_t$ against time) for an experiment with $P_1 = 15.90$ Torr and $M_s = 2.247$. $T_5 = 1285$ K, $\rho_5 = 2.668 \times 10^{18}$ molecules cm^{-3}, $[C_2H_2]_0 = 2.156 \times 10^{14}$ molecules cm^{-3}, and $[C_2D_5I]_0 = 1.624 \times 10^{12}$ molecules cm^{-3}. The line is a simulation with a 41 step mechanism (from ref 10 and including the title reaction), and the fitted second order value for k_{bH} is 3.0×10^{-11} cm^3 $molecule^{-1}$ s^{-1}.

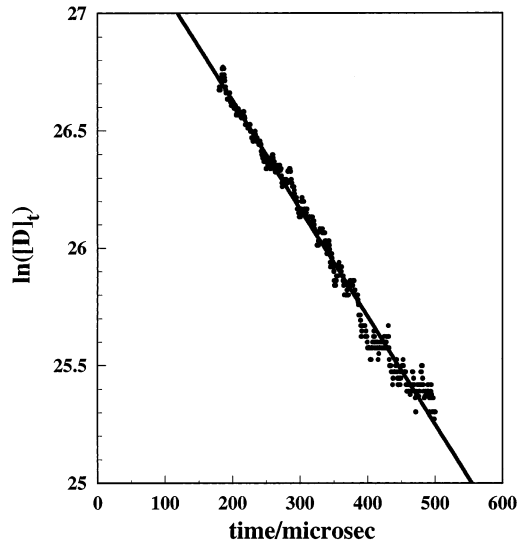

Figure 3. First-order plot for the experiment shown in Figure 1 (i.e., $\ln([D]_t)$ against time). The negative slope of the line gives the decay constant, 4684 s^{-1}, and $k_{bD} = k_{first}/[C_2H_2]_0 = 2.53 \times 10^{-11}$ cm^3 $molecule^{-1}$ s^{-1}.

atom depletion experiments using first-order analysis are given in Table 1. Complete simulations were necessary in four of the lower temperature experiments where D formation becomes comparable to depletion rates. H atom profiles were likewise fitted with the mechanism for the H atom formation experiments listed in Table 2, and the solid line in Figure 2 shows such a simulation. In this case, we elected to simulate the entire set of experiments giving the listed k_{bH} values. As expected, first-order buildup plots (i.e., $\ln\{([H]_\infty - [H]_t)/[H]_\infty\}$ against time) also gave k_{bH} values that were the same as those from the complete simulations within experimental error.

Figure 4 shows an Arrhenius plot of the data from Tables 1 and 2 where the solid and open points are k_{bD} and k_{bH}, respectively. The sets can be analyzed individually giving Arrhenius expressions over the T range, 1100−1630 K

$$k_{bD} = (1.83 \pm 0.39) \times 10^{-10} \exp(-2552 \pm 273\ \mathrm{K/T}) \quad (5)$$

and

$$k_{bH} = (4.07 \pm 0.78) \times 10^{-10} \exp(-3519 \pm 251\ \mathrm{K/T}) \quad (6)$$

TABLE 1: D-Atom ARAS High Temperature Rate Data for D + C_2H_2 → C_2HD + H

P_1/Torr	M_s[a]	$\rho_5/(10^{18}$ cm$^{-3})$[b]	T_5/K[b]	k_{first} /s^{-1}	k_{bD}/(cm^3 s^{-1})[c]
$X_{C_2D_5I} = 8.668 \times 10^{-7}$ $X_{C_2H_2} = 2.939 \times 10^{-4}$					
5.94	2.270	1.024	1318	7512	2.50(−11)[d]
5.95	2.189	0.985	1236	sim.	2.10(−11)
10.95	2.435	2.017	1486	18875	3.18(−11)
10.96	2.174	1.785	1213	10293	1.96(−11)
$X_{C_2D_5I} = 8.036 \times 10^{-7}$ $X_{C_2H_2} = 1.040 \times 10^{-4}$					
5.97	2.444	1.112	1505	3894	3.37(−11)
5.96	2.290	1.037	1339	3157	2.93(−11)
5.98	2.271	1.032	1320	2787	2.60(−11)
5.99	2.250	1.023	1298	2511	2.36(−11)
5.97	2.552	1.159	1629	4400	3.65(−11)
10.97	2.243	1.852	1282	4864	2.53(−11)
10.95	2.112	1.723	1152	sim.	2.50(−11)
10.94	2.172	1.779	1210	3772	2.04(−11)
10.95	2.387	1.977	1433	5996	2.91(−11)
10.91	2.480	2.047	1536	9048	4.25(−11)
$X_{C_2D_5I} = 6.087 \times 10^{-7}$ $X_{C_2H_2} = 8.082 \times 10^{-5}$					
15.95	2.181	2.587	1219	4866	2.33(−11)
15.95	2.132	2.526	1167	sim.	2.20(−11)
15.96	2.091	2.461	1132	sim.	2.00(−11)
15.95	2.234	2.659	1272	4853	2.26(−11)
15.88	2.325	2.767	1366	6461	2.89(−11)
15.87	2.391	2.848	1437	6882	2.99(−11)
15.89	2.448	2.921	1500	8551	3.62(−11)

[a] The error in measuring the Mach number, M_s, is typically 0.5−1.0% at the one standard deviation level. [b] Quantities with the subscript 5 refer to the thermodynamic state of the gas in the reflected shock region. [c] Rate constants for reaction 1 using first-order analysis as described in the text. [d] Parentheses denotes the power of 10.

TABLE 2: H-Atom ARAS High Temperature Rate Data for D + C_2H_2 → C_2HD + H

P_1/Torr	M_s[a]	$\rho_5/(10^{18}$ cm$^{-3})$[b]	T_5/K[b]	k_{bH}/(cm^3 s^{-1})[c]
$X_{C_2D_5I} = 8.668 \times 10^{-7}$ $X_{C_2H_2} = 2.939 \times 10^{-4}$				
5.96	2.318	1.051	1368	3.2(−11)[d]
5.97	2.055	0.916	1106	1.4(−11)
10.92	2.235	1.836	1274	2.8(−11)
10.89	2.171	1.771	1210	2.0(−11)
$X_{C_2D_5I} = 8.036 \times 10^{-7}$ $X_{C_2H_2} = 1.040 \times 10^{-4}$				
5.96	2.389	1.085	1445	3.4(−11)
5.94	2.538	1.147	1612	4.2(−11)
5.95	2.400	1.088	1456	3.1(−11)
5.8	2.377	1.050	1432	3.2(−11)
5.86	2.321	1.035	1372	3.0(−11)
5.94	2.259	1.019	1308	2.4(−11)
10.93	2.219	1.823	1258	2.5(−11)
10.94	2.264	1.866	1303	2.9(−11)
10.95	2.251	1.855	1290	2.7(−11)
10.93	2.184	1.790	1223	2.3(−11)
10.88	2.240	1.834	1279	2.6(−11)
10.96	2.040	1.651	1084	1.6(−11)
10.89	2.115	1.717	1156	2.1(−11)
$X_{C_2D_5I} = 6.087 \times 10^{-7}$ $X_{C_2H_2} = 8.082 \times 10^{-5}$				
15.92	2.520	3.010	1581	4.8(−11)
15.90	2.436	2.908	1486	3.9(−11)
15.87	2.393	2.851	1439	3.9(−11)
15.90	2.247	2.668	1285	3.0(−11)
15.96	2.252	2.677	1295	3.0(−11)
15.98	2.292	2.732	1336	2.9(−11)
15.88	2.208	2.604	1250	2.7(−11)

[a] The error in measuring the Mach number, M_s, is typically 0.5−1.0% at the one standard deviation level. [b] Quantities with the subscript 5 refer to the thermodynamic state of the gas in the reflected shock region. [c] Rate constants for reaction 1 using mechanism simulations of $[H]_t$ formation as described in the text. [d] Parentheses denotes the power of 10.

both in units of cm^3 $molecule^{-1}$ s^{-1}. Because of the relatively small range in T^{-1} space with attendant scatter, the equations appear to differ; however, the sets overlap with one another within combined one standard deviations. Including all points

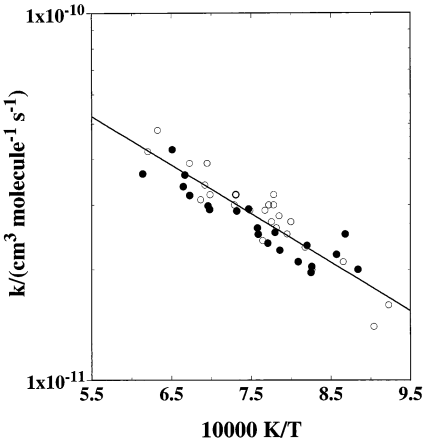

Figure 4. Arrhenius plot of the data from Tables 1 and 2. (●) D-atom experiments. (○) H-atom experiments. The line is the linear-least squares result, eq 7, that includes all data points.

from Tables 1 and 2, the combined Arrhenius expression in the same units is then

$$k_b = (2.77 \pm 0.45) \times 10^{-10} \exp(-3051 \pm 210\ \mathrm{K/T}) \quad (7)$$

The linear-least-squares result described by eq 7 is plotted in Figure 4. The one standard deviation of the points from the line in the figure is ±10.7%. Our conclusion is therefore that $k_{bD} = k_{bH}$ over the present range of temperatures and pressures. This is a significant conclusion because, in contrast to eq 4, the RRKM expression for H-atom formation is

$$k_{bH} = k_{1D\infty} \int_{\epsilon_0}^{\infty} (k_{f\epsilon}/(k_{f\epsilon} + k_{b\epsilon} + \beta\omega) f(\epsilon) d\epsilon \quad (8)$$

Equal rate constants for k_{bD} and k_{bH} are strong evidence that stabilization is negligible in comparison to either forward or backward dissociation of $C_2H_2D^*$. Then, $k_{bH} = k_{1D\infty}\langle k_{f\epsilon}/(k_{f\epsilon} + k_{b\epsilon})\rangle = k_{bD}$.

Discussion

There are no previous high-temperature studies of the title reaction. There are however lower temperature studies, obtained with the discharge flow[3,5] and pulse radiolysis-ARAS[6] techniques, the latter being carried out at atmospheric pressure. The low-temperature result of Hoyermann et al.[3] follows the Arrhenius expression

$$k_b = 5.15 \times 10^{-11} \exp(-1862\ \mathrm{K/T}) \quad (9)$$

implying a value at room temperature of $\sim 1 \times 10^{-13}$ cm^3 molecule^{-1} s^{-1}. The room-temperature result of Keil et al.[5] is 1.2×10^{-13}, whereas the value from Sato and co-workers[6] is 2.2×10^{-13} cm^3 molecule^{-1} s^{-1}. As discussed below, the data from Sato and co-workers are difficult to reconcile and therefore will not be further considered. In the low-T studies, the rate constant being measured is probably >85% of the high-pressure limit.

Theory. There have been a number of previous theoretical studies on both the rate constant and the isotope effects for the addition of hydrogen atoms to acetylene. These include calculations reported in the original experimental papers,[5,6] more extensive calculations without experimental results,[8] and recent calculations accompanying an experimental study of vinyl-radical dissociation.[9] All of these previous studies used a conventional RRKM model[20] (eqs 3, 4, and 8) for the kinetics where the critical points on the potential energy surface were characterized either by adjusted parameters to fit experiment or by ab initio electronic structure calculations. In this study, we will continue to use an RRKM model for the kinetics but test eight different but popular electronic structure methods for characterizing the potential energy surface and also examine the impact of variational effects and sophisticated tunneling models on the reaction rate constants. First the electronic structure results will be discussed, and then the kinetics variations and final results will be presented.

Electronic Structure Calculational Details. The stationary points for this reaction were characterized with eight different levels of electronic structure theory. These include calculations using four versions of density function theory (DFT), two variants of Gaussian-3 theory, one coupled-cluster theory, and a multireference configuration interaction theory.

The versions of DFT theory used were B3LYP/6-31+G(d,p), BH&HLYP/6-31+G(d,p), MPW1K, and MPW−SRP (a DFT optimized for this specific reaction as described below). All of the DFT calculations were carried out using the Gaussian 98 program.[21] The B3LYP and BH&HLYP are standard options in Gaussian 98 and need not be described further.

MPW1K is a DFT model developed by Lynch et al.[22] specifically for the purpose of performing kinetics calculations. The starting point for this approach was the MPW1PW91 model proposed by Adamo and Barone.[23] In this approach one can write a hybrid Fock-Kohn−Sham operator as follows:

$$F = F^{H} + C_X^{HF}F_X^{HF} + C_X^{S}F_X^{S} + C_X^{MPW}F_X^{MPW} + C_C^{L}F_C^{L} + C_C^{NL}F_C^{NL} \quad (10)$$

where F^H is the Hartree operator, F_X^{HF} is the Hartree−Fock exchange operator, F_X^{MPW} is the Slater local density functional for exchange, F_X^S is the modified Perdew-Wang 1991 gradient correction for the exchange functional, and F_C^L and F_C^{NL} are the local and nonlocal parts of the Perdew-Wang 1991 correlation function. This Hamiltonian has a total of five parameters, C_X^{HF}, C_X^S, C_X^{MPW}, C_C^L, and C_C^{NL}. In the original MPW1PW91 model[23] the parameters are defined as follows, $C_X^{HF} = 0.25$, $C_X^S = C_X^{MPW} = 0.75$ ($=1 - C_X^{HF}$), and $C_C^L = C_C^{NL} = 1.0$. In the MPW1K[22] model, a one-parameter optimization is carried out in order to fit the energetics (barrier heights and energies of reaction) for 20 abstraction reactions. The parameters used in the MPW1K model are the following: $C_X^{HF} = 0.428$, $C_X^S = C_X^{MPW} = 0.572$ ($=1 - C_X^{HF}$), and $C_C^L = C_C^{NL} = 1.0$.

As will be described below, use of the MPW1K potential surface did not lead to satisfactory agreement with either higher level electronic structure theory or with measured rate data for this reaction. Two attempts were made to improve the agreement. First, a one-parameter re-optimization of the functional was performed (exactly analogous to the optimization done in the original MPW1K method). This did not lead to a significant improvement with the higher level electronic structure theory. The second attempt involved independently optimizing all five of the above parameters. The parameters were optimized to minimize the sum of the squares of the percentage errors in the DFT barrier height, reaction exothermicity, and the location of the barrier (as measured by the C−H distance). The reference values used in this optimization were the results of CCSD(T)/aug-cc-pvtz calculations described below. The resulting parameters are as follows: $C_X^{HF} = 0.19$, $C_X^S = 0.9$, $C_X^{MPW} = 0.1$, $C_C^L = 0.0$, and $C_C^{NL} = 1.1$. We denote this functional MWP−SRP to indicate that the parameters have been optimized for a specific reaction.

TABLE 3: Calculated Imaginary Frequencies, Barrier Heights, and Reaction Exothermicities for H+HCCH → H_2CCH[a]

method	imaginary frequency (cm^{-1})	barrier height (kcal/mol) un-adjusted	barrier height (kcal/mol) adjusted	reaction exothermicity (kcal/mol)
HF/6-31G(d,p)[b]		5.23		−48.04
MP2/6-31G(d,p)[b]	1562	17.36		−30.17
MP4/6-31G(d,p)[b]	1388	13.08		−35.24
PMP4/6-31G(d,p)[b]	1051	6.40		−40.07
B3LYP/6-31+G(d,p)	541	1.08(1.57)	3.56(4.03)	−47.46(−41.35)
BH&HLYP/6-31+G(d,p)	714	2.19(2.65)	3.82(4.26)	−49.56(−43.34)
MPW1K	730	2.75(3.20)	3.87(4.29)	−50.22(−44.00)
MPW−SRP	866	3.78(4.26)	4.06(4.53)	−41.60(−35.54)
G3	946	2.83(2.24)	5.32(4.73)	−40.41(−35.21)
G3//B3LYP	524	1.89(2.49)	3.37(3.99)	−40.85(−34.76)
CCSD(T)/aug-cc-pvtz	862	3.78(4.44)	3.87(4.52)	−41.20(−34.90)
CCSD(T)/aug-cc-pvqz		3.79		−40.96
CAS+1+2/aug-cc-pvtz	969	5.37(5.96)		−38.18(−31.81)
CAS+1+2/aug-cc-pvqz		5.47		−37.81
CAS+1+2+QC/aug-cc-pvtz	895	4.16(4.60)	4.15(4.59)	−40.33(−34.19)
CAS+1+2+QC/aug-cc-pvtq		4.20		−39.99

[a] Numbers in parenthesis include zero-point energy. [b] From ref 9.

The two Gaussian-3 models used are the original G3[24] method and a newer variant denoted G3//B3LYP.[25] There are differences between these methods in both the geometries and frequencies. In the original G3 model,[24] the geometries come from second-order perturbation theory, MP2/6-31G(d), and the frequencies from scaled Hartree−Fock theory, HF/6-31G(d), with a scale factor of 0.8929. In the newer G3//B3LYP model,[25] both the geometries and frequencies come from B3LYP/6-31G(d) calculations with the frequencies scaled by a factor of 0.96.

Two sets of large-scale ab initio calculations have also been carried out, one using a coupled-cluster method and the other using multireference configuration interaction. Both sets of calculations were done using the MOLPRO package of codes,[26] and both employ the Dunning augmented correlation consistent basis sets.[27−29] Geometry optimizations and frequency analyses were done using the triple-ζ, aug-cc-pvtz, basis set, and single-point calculations were done using the larger quadruple-ζ, aug-cc-pvqz, basis set. The coupled-cluster calculations employ the open shell, spin unrestricted, coupled cluster theory (restricted to single and double excitations with perturbative triple excitations) of Knowles et al.,[30] CCSD(T). The multireference configuration interaction calculations start with a five electron − five orbital CASSCF calculation[31,32] in which the active orbitals consist of the acetylenic π and π^* orbitals and the hydrogen 1s orbital. The internally contracted configuration interaction calculations[33,34] then include all single and double excitations relative to this reference wave function. A multi-reference Davidson correction[35,36] was added to yield the final CAS+1+2+QC energies.

Electronic Structure Calculational Results. The calculated barrier heights and reaction exothermicities are summarized in Table 3 along with earlier results from ref 9. The present zero-point corrected barrier heights fall into three distinct groups, low, intermediate, and high. The low barriers (i.e., those less than 3.5 kcal mol^{-1}) include all of the DFT methods (except MPW−SRP) and both G3 methods. The CAS+1+2 calculations (without the Davidson correction) give barriers that are noticeably higher (>5.0 kcal mol^{-1}) than any of the other methods. The CAS+1+2+QC, the CCSD(T), and the MPW−SRP (which is fit to CCSD(T)) barrier heights are clustered in the range 4.2−4.6 kcal mol^{-1}. The small differences between the barrier heights obtained with the aug-cc-pvtz basis set and the single-point calculations with the aug-cc-pvqz basis set suggest that these results are well converged with respect to the one electron basis set.

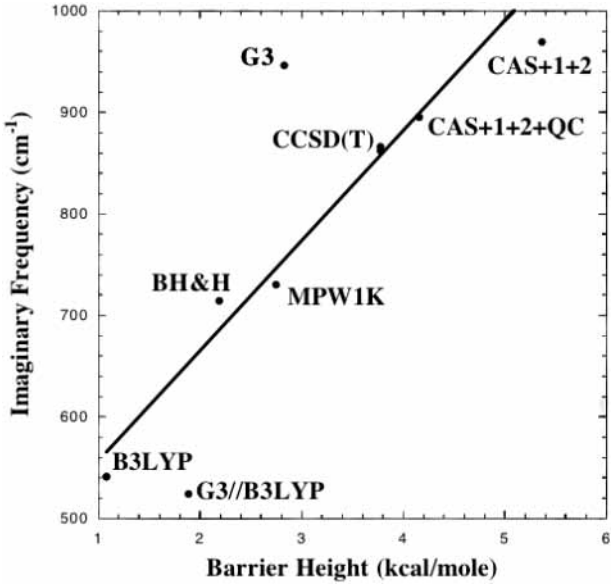

Figure 5. Plot of calculated imaginary frequencies vs barrier heights for the eight electronic structure methods. The solid line is a linear-least-squares fit.

The calculated zero-point corrected reaction exothermicities range from −31.8 (CAS+1+2) to −44.0 kcal mol^{-1} (MPW1K) with the two highest level models, CCSD(T) and CAS+1+2+QC, giving −34.9 and −34.2 kcal mol^{-1}, respectively. The single-point calculations with the aug-cc-pvqz basis set decrease both of these exothermicities slightly yielding our best theoretical estimates of −34.7 to −33.8 kcal mol^{-1} for CCSD(T) and CAS+1+2+QC, respectively. The best available experimental estimate for this quantity is −33.5 ± 0.9 kcal mol^{-1}.[37] With the exception of MPW−SRP all of the density functional methods yield exothermicities that are 8−10 kcal mol^{-1} too large, whereas the G3 models are in reasonable agreement with both the higher level calculations and experiment.

Also shown in Table 3 are the calculated imaginary frequencies. There is a rough linear relationship (see Figure 5) between the barrier heights and the imaginary frequencies except for the G3 methods. The imaginary frequency from the original G3 method falls significantly above, and the G3//B3LYP frequency falls significantly below, the near linear correlation observed in the other methods. This behavior is not unexpected because the G3 frequencies come from a different level of theory than

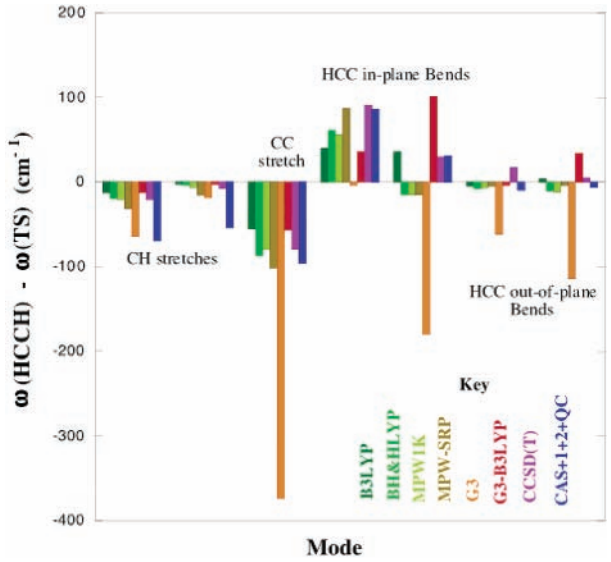

Figure 6. Change in the seven conserved mode frequencies between the reactant and transition-state for H + HCCH → H_2CCH for each of the eight electronic structure methods.

the G3 energies. The kinetics consequences of these differences will be discussed below.

The eight electronic structure methods also show some significant differences for the seven conserved modes in this reaction. Figure 6 shows a plot of the changes in each of the seven conserved modes between the reactant and transition-state for each of the eight methods. The three modes on the left are the CH and the CC stretches. All levels of theory predict decreases in these three modes between acetylene and the transition-states as would be expected (the CC bond is in transition from a triple bond to a double bond and the hybridization of the CH bonds is changing from sp to sp^2). The two modes on the right are the out-of-plane bends. All levels of theory except the G3 models predict only small changes in these bends. The remaining two modes in the middle of the plot are where the most striking differences between the models occur. These are the in-plane HCC bends. The highest level theories, CCSD(T) and CAS+1+2+QC, show significant increases in both of these bends, whereas BH&HLYP, MPW1K, and MPW−SRP all show significant decreases in one of these two modes and smaller increases in the other.

Kinetics Calculations. Intrinsic reaction path calculations were done for both H + HCCH and D + HCCH using the MPW−SRP electronic structure method. This allows the high-pressure limiting addition rate constants for both reactions to be determined by variational transition state theory (VTST)[38] as embodied in the POLYRATE[39] software. Such calculations can be used to determine the extent of both variational effects and sophisticated tunneling processes in the addition process. Variational effects include entropic as well as energetic considerations in the location of the reaction bottleneck along the reaction path. Conventional TST, as used in all previous theoretical studies as part of the RRKM model, includes only energetic effects that restrict the reaction bottleneck location to the saddle point on the reaction path for all temperatures. Improved canonical variational transition state theory (ICVT) calculations determine temperature-dependent variational effects and, as embodied in POLYRATE, determine the reaction bottleneck displacement from the saddle point in the mass weighted reaction coordinate, *s*. Tunneling calculations in POLYRATE go beyond both the Wigner approximation and the Eckart approximation used in previous theoretical studies

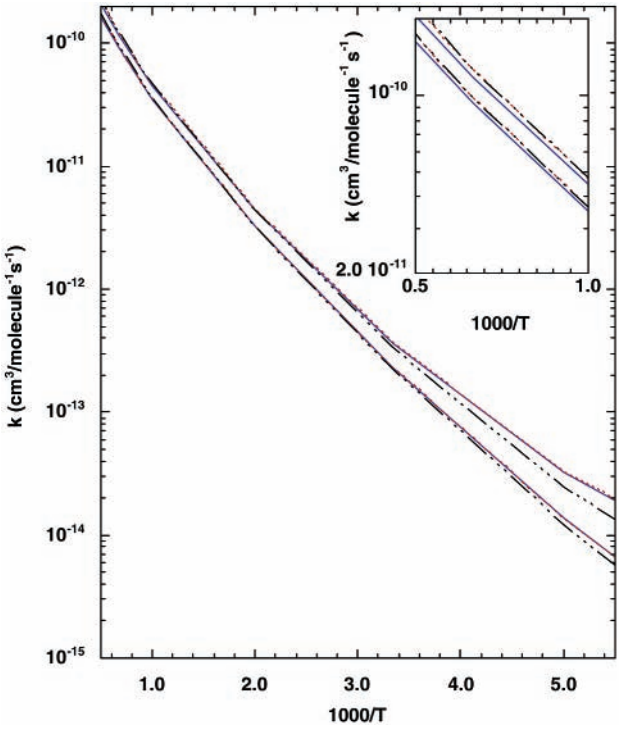

Figure 7. Computed high-pressure rate constant versus temperature. Top (bottom) set of three curves are for H(D) + HCCH using the MPW−SRP characterization of the reaction path. The three curves of each set are computed according to the following kinetics methods: —, ICVT/SCT; ···, TST/SCT; and − · −, TST/Eckart.

(refs 8 and 9, respectively) to the small curvature tunneling (SCT) model that uses the actual shape of the reaction path.[38]

Figure 7 displays the results of the VTST calculations with POLYRATE on the MPW−SRP surface. The computed high-pressure limiting rate constant versus inverse temperature is plotted for H + HCCH (upper curves) and for D + HCCH (lower curves). For each reaction, there are three separate calculations: TST/SCT, ICVT/SCT, and TST/Eckart. Comparing the first two calculations for either isotopic combination, the variational lowering of the computed rate constant is small (<10% (7%) for H(D) + HCCH) and is essentially confined to high temperatures (>1000 K). Consequently, conventional RRKM calculations, as used in the past, can be applied to all eight electronic structure characterizations of the addition potential energy surface, and the computed over estimations of the rate constants due to variational effects are not expected at the higher temperatures of the experiments to exceed ∼5%.

Figure 7 also allows an evaluation of tunneling methods. Knyazev and Slagle[9] were the first to incorporate an Eckart model for tunneling. Following Marcus and Coltrin,[40] the Eckart potential is fit to $V_a^G(s)$, the ground state vibrationally adiabatic potential, or in other words, $V_{MEP}(s)$ corrected for the change in zero-point energy from the reactants. Given the imaginary frequency and the zero-point corrected barrier height in both the addition and dissociation directions, an Eckart potential as a function of *s* can be determined. Then, an energy-dependent analytic Eckart tunneling probability can be incorporated[41] into an energy-dependent sum of states $N(E)$ which with proper convolution over temperature-dependent translational energy distributions can lead to either TST/Eckart rate constants (as in Figure 7) for the high-pressure limit or RRKM/Eckart pressure-dependent rate constants. As the results show, the TST/Eckart agreement with TST/SCT is quite good with maximum errors of 35% (16%) for H(D) + HCCH at the very lowest temper-

atures of ~200 K. Furthermore, for both isotopic combinations, comparison of the MPW−SRP $V_a^G(s)$ with the Eckart fit shows a close similarity with the Eckart model being slightly too broad. Slightly increasing the imaginary frequency by 8% (5%) for H(D) + HCCH produces a TST/adjusted-Eckart rate constant that has maximum relative errors of less than 3% from TST/SCT and is indistinguishable from the TST/SCT results from POLYRATE in Figure 7. This modest scaling in the imaginary frequency will be used with all other electronic structure calculations to produce RRKM/adjusted-Eckart rate constants for all temperatures and pressures.

The remaining features of the conventional RRKM calculations are as follows. All species (acetylene, the saddle point, and the vinyl radical) are treated as harmonic oscillator rigid rotors as characterized by the electronic structure calculations (e.g., see Tables 1S−8S for the cases considered here). As in previous theoretical studies,[8,9] the external rotation with the smallest moment of inertia is presumed to be active in exchanging energy with the vibrational modes. Pressure dependence is treated in the weak collision approximation[42] using an energy gap model and standard estimations for the gas kinetic collision rate to describe the relaxation of the chemically activated vinyl-radical by the buffer gas.[43] Numerous buffer gases have been used in the experimental studies; however, in the present calculations, only He will be considered. Our experimental study uses Kr as a buffer gas, but as described in the Introduction, very little pressure dependence is expected for the D + HCCH combination. Most experiments at lower pressures on other combinations used He. Rigorously, RRKM calculations require a convolution over both energy and angular momentum. However, tests confirm the expectation that for this reaction the convolution over angular momentum can be replaced with negligible error by a temperature dependent average of the angular momentum. Hence, all RRKM calculations are done with only an energy convolution.

The details of the energy gap model describing inelastic transition probabilities in collisions between the buffer gas and the chemically activated vinyl radical are as yet unspecified. The major focus of this theoretical study is the D + HCCH isotopic combination where very little pressure dependence is expected. Consequently, little attention to details of the energy gap model is required. However, such is not the case for H + HCCH. Here, several experimental studies are available[4−7] which appear to show pressure-dependent results converging on apparent high-pressure limits at pressures below 760 Torr over a temperature range up to ~500 K. These results were resistant to theoretical analysis when they were first published.[5] A subsequent theoretical analysis[8,9] has largely re-affirmed this situation with the most recent calculation by Knyazev and Slagle[9] obtaining only qualitative agreement with the measured pressure dependence that leads to a systematically higher computed high-pressure limit than the experiments at ~400 K. Although this will not be discussed in detail, our most reliable calculations will not materially change this conclusion. To model in detail the pressure dependence down toward the low-pressure limit requires parametric studies of energy gap models and perhaps the replacement of the weak collision approximation by master equation studies[20] (all of which Knyazev and Slagle[9] performed). Instead, we will attempt to compare our results only with the highest pressure measurements of H + HCCH which are near enough to the high-pressure limit to again require only modest attention to the details of the energy gap model. Throughout our calculations, we will characterize our energy gap model by a temperature-independent $\Delta E_{all} = -100$ cm^{-1} which is of the right qualitative scale in comparison to more detailed studies.

One other issue remains regarding the comparison of the theory to experiment. One series of measurements by the Sato group[6a,b] on various isotopic combinations of H + HCCH is high relative to other measurements on identical isotopic combinations. These measurements have been criticized (e.g., see Knyazev and Slagle[9]) by suggesting that stoichiometric effects were not properly taken into account. Our calculations also are not consistent with this series of measurements, and the details of the disagreement will not be explicitly discussed.

The above discussion motivates a comparison of the computed RRKM/adjusted-Eckart kinetics of eight different electronic structure calculations with the D + HCCH measurements presented in this paper, with those of Hoyermann et al.,[3] and those of Keil et al.,[5] and, for H + HCCH, with the highest pressure measurements of Payne and Stief,[4] Keil et al.,[5] and Ellul et al.[7] The temperature range of these measurements stretches from 193 K (for Payne and Stief) to 1629 K (here).

Without scaling, any straightforward comparison between theory and experiment is dominated by the experimental results at the lowest temperatures. Here, the range in computed barriers (from 1.07 (B3LYP) to 4.20 kcal mol^{-1} (CAS+1+2+QC)) guarantees multiple order of magnitude variations in the computed rate constant. On this basis alone, only three electronic structure methods are consistent with experiment: CCSD(T), MPW−SRP, and CAS+1+2+QC. The other five methods produce rate constants very much too high at the lowest temperatures because their computed barriers are too low by at least 1 kcal mol^{-1}. However, in most comparisons between theory and experiment, some adjustment of the computed barrier can be explored because this is a difficult value to directly compute with high confidence.[44] Consequently, for a more stringent test between all of the methods, the addition barrier for each method was adjusted to reproduce the 193 K measured high-pressure limit of Payne and Stief for H + HCCH. However, before such scaling can be carried out, the question of frequency scaling must also be addressed. Four of the methods (B3LYP, BH&HLYP, MPW1K, and MPW−SRP) have parameters within the density functional whose values are adjusted to reproduce raw energies derived by other means. However, all four of these methods have additional frequency scaling approximations that improve agreement with experimental frequencies[45] or with frequencies derived from high level ab initio calculations.[46] Although it makes a minor difference to the overall kinetics results, both frequencies and subsequent energies have been scaled for each method when applicable. The resulting energy changes in the computed barrier, to obtain agreement between theory and experiment at 193 K for the H + HCCH high-pressure limit, are listed in Table 3 along with the final scaled barrier. As the table indicates, both G3 methods and all of the density functional methods except MPW−SRP involve barrier adjustments of >1 kcal mol^{-1}. However, the three methods based on either CCSD(T) or CAS+1+2+QC for their barrier heights involve adjustments of ~0.1 kcal mol^{-1}. The final scaled barriers are all within 0.5 kcal mol^{-1} from each other. Although not listed in the table, the zero-point corrected barriers are even closer together with a spread of only 0.3 kcal mol^{-1}.

The eight separate RRKM/adjusted-Eckart rate constant calculations approximately fall into three groups. One member of each group is represented in Figures 8−10. Each of these three figures contains computed rate constants as a function of T^{-1} for H + HCCH and for D + HCCH. In each case, the two computations for H + HCCH are (a) the high-pressure limit

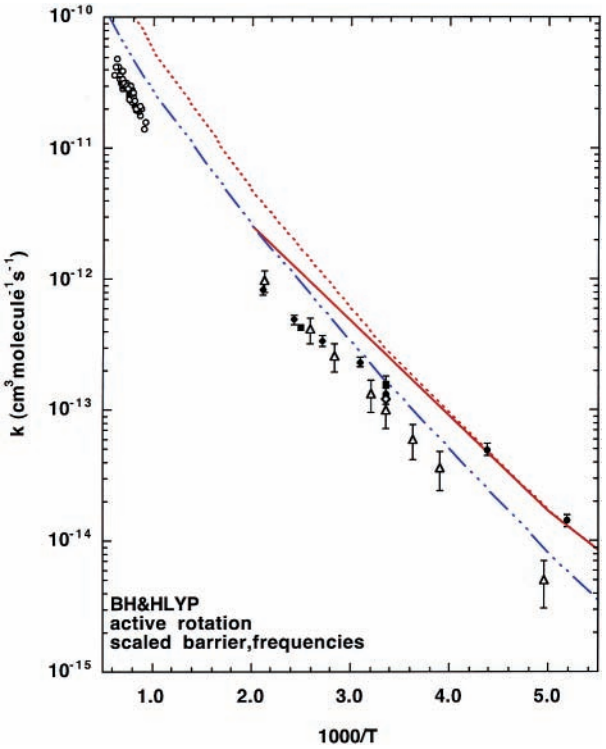

Figure 8. Rate constant for H(D) + HCCH versus inverse temperature. Experimental results H+HCCH are in solid symbols: ●, Payne et al.; ♦, Ellul et al.; and ■, Kiel et al. Experimental results in D+HCCH are in open symbols: ◊, Kiel et al.; △, Hoyermann et al.; and ○, present measurements. The computed BH&HLYP rate constants are: − ··· −, D+HCCH at 6 Torr He; —, H+HCCH at 760 Torr He; and ···, H+HCCH at the high-pressure limit.

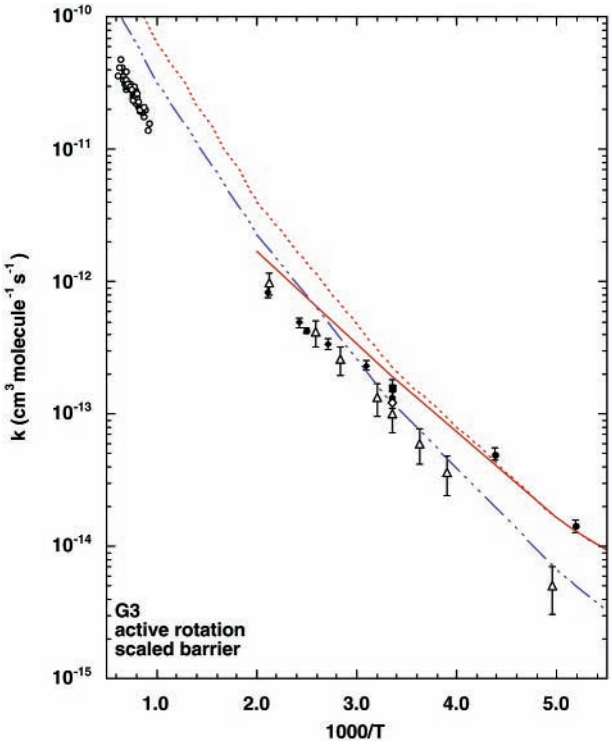

Figure 9. As in Figure 8 only for G3 rate constants.

and (b) the computed rate constant at 760 Torr. The highest measured rate constants for H + HCCH are represented as closed symbols in the figure and correspond to pressures between 700 and ~760 Torr in He. The computed rate constants for D + HCCH are for 6 Torr, while the open symbols indicate the measured rate constants of pressures from 6 to 760 Torr. The computed rate constants for all eight electronic structure methods share two characteristics that are consistent with the experimental results in Tables 1 and 2 for D + HCCH. All calculations show negligible pressure dependences from 6 to 760 Torr over the full range of temperatures in the experimental record, and the rates for D-atom loss and H-atom gain are essentially equal. For H + HCCH, all calculations also show, in agreement with the measurements of Payne and Stief,[4] that the high-pressure limit has been reached with 760 Torr He at the lowest temperature, 193 K.

Figure 8 is representative of the group of four calculations that are in poorest agreement with experiment. This group includes B3LYP, G3-B3LYP, BH&HLYP, and MPW1K. The BH&HLYP computed rate constants are displayed in the figure. As the figure indicates, at all temperatures, the computed rate for D + HCCH is substantially too high. Similarly, at the higher temperatures of the experimental record, the computed rate for H + HCCH at 760 Torr is too high. As seen in Table 3, this group involved the largest energy scaling. Consistent with low directly computed barriers, this group had the lowest imaginary frequencies. Consequently, at the lowest temperatures where tunneling dominates, there is insufficient tunneling which leads to too small a computed change between H + HCCH and D + HCCH. The adjusted barrier by design compensates for weak tunneling at 193 K by being too low. At higher temperatures, where tunneling is less important, this overly low barrier leads to rate constants that are too high relative to the experiment.

Figure 9 represents the computed results for the G3 method. This method paradoxically produces the highest imaginary frequencies of any method but a directly computed barrier that is too low by ~1 kcal mol^{-1} (see Table 3). Consequently, the computed results display reasonable agreement with the lowest temperature results for both H + HCCH and D + HCCH. The computed rates tend to veer upward from the measured results for both isotopic combinations in the middle range of temperatures (~400 K) but the disagreement is not too substantial. However, at the highest temperatures of the D + HCCH measurements in this paper, the computed results are substantially high by more than a factor of 2.

Figure 10 represents the computed results for a group of three methods: CCSD(T), MPW−SRP, and CAS+1+2+QC. All three of these methods at their core use higher level electronic structure methods than any of the other five methods. As seen in Table 3, these three methods require very minor adjustments in the barrier to anchor the computed rate constants to the lowest temperature measurement. The CCSD(T) results in the figure agree with the highest pressure H + HCCH measurements over the whole temperature range of the experimental record. The D + HCCH computed rate constants are consistent with the previous measurements except at the highest temperatures (~500 K) where they are somewhat high. The computed rate constants are slightly higher than the measured results from the present study and in much better agreement than the computed results in Figures 8 and 9 for the two other groups of calculations. Although the CAS+1+2+QC and CCSD(T) barriers differ by ~0.3 kcal mol^{-1} (see Table 3), small changes in the frequencies make the CAS+1+2+QC rate constants nearly indistinguishable from those for CCSD(T) in Figure 10. The MPW−SRP method, which is keyed to the CCSD(T) results, produces rates that at the highest temperatures ride higher than the results in Figure 10 by about the thickness of the plotted line.

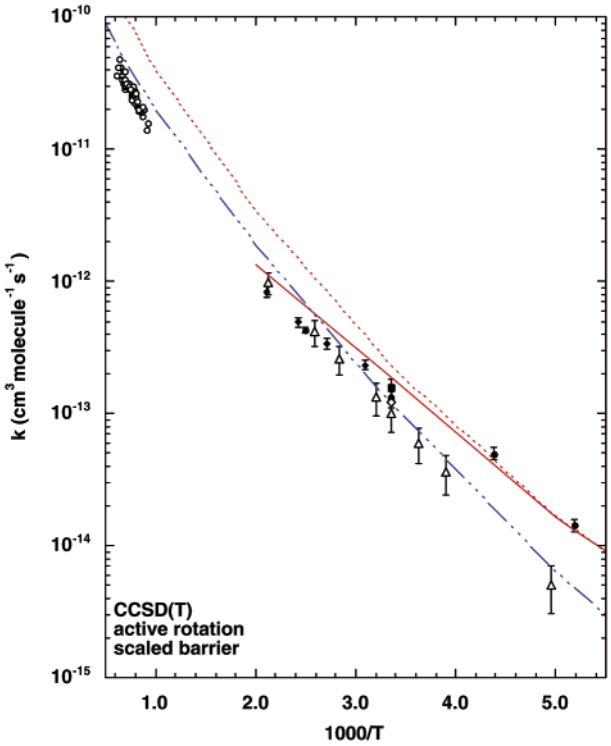

Figure 10. As in Figure 8 only for CCSD(T) rate constants.

Much of the above discussion of Figures 8−10 is concerned with the full temperature range in the experimental record. However, a more focused discussion is necessary to understand why the different electronic structure methods produce noticeably different results for the higher temperature measurements on the D + HCCH reaction reported in this paper. Because only one of the two competing routes for the dissociation of the HDCCH activated complex leads to products, it could be possible that the different electronic structure methods describe the competition differently leading to different rate constants. This can be tested by comparing the ratio of the computed rate constant at finite pressure with the computed rate constant in the high-pressure limit (where all activated complexes are converted to products). For any temperature in the range relevant to the measurements in Tables 1 and 2, all eight methods give computed ratios that differ from each other by less than ±1%. All eight methods show that approximately 60% of the activated complexes are converted to products over the temperatures of the experiment; i.e., $\langle k_{f\epsilon}/(k_{f\epsilon}+ k_{b\epsilon})\rangle = 0.6$ as anticipated in the Introduction. This fraction is even higher at lower temperatures.

If different descriptions of competition are not a factor, then the eight methods must differ in the rate of complex formation; i.e., in the high-pressure limit of the D + HCCH addition rate constant, $k_{1D\infty}$. At the temperatures of the measurements, D-atom tunneling is inconsequential. Consequently, the kinetic differences of the eight methods reside in the computed structures, frequencies, and energetics of the HCCH reactant and the D−HCCH transition-state. Because the structures are essentially the same for all of the methods, only differences in the computed barrier height and frequencies drive the kinetics differences. Unfortunately, there is no one dominating trend to explain all eight differences. Although the size of the computed rate constant is generally inversely related to the barrier height, G3 has one of the higher computed rate constants (see Figure 9) but also has the highest zero-point corrected adjusted D + HCCH barrier height (as is also found in Table 3 for the H + HCCH barrier height). Figure 6 indicates the large differences between methods caused by computed frequency changes from the reactants to the transition-state. In part, G3 gives such a high rate constant, despite having a high barrier, because (as indicated in Figure 6) its transition-state frequencies are so low relative to the reactants. Finally, the computed acetylene frequencies, the lowest of which varies from 512 cm^{-1} (G3-B3LYP) to 709 cm^{-1} (G3), have a substantial impact on the kinetics calculations. Typically, one uses computed, instead of measured, harmonic frequencies for reactants in the hope that some cancellation of error will occur because differences between reactant and transition-state frequencies are important in the structure of the kinetics theory. Although in general low frequencies for HCCH act to lower the rate constants, the highest computed rate constant is produced from the method with the lowest low frequency for HCCH (G3-BLYP). Given the difficulty of sorting out trends, all that can be said is that the best methods of CCSD(T), CAS+1+2+QC, and MPW−SRP have the right combination of energetics and frequencies to make the best contact with experiment.

At the scale of disagreement shown in Figure 10, some small effects have been neglected in the computed rate constants that can quantitatively change the comparison between experiment and theory. As mentioned, all of the high temperature computed results in Figures 8−10 neglect variational effects and therefore over estimate the true rate constant. However, these effects are only about 4−5% over the temperature range of the D + HCCH experiments in Tables 1 and 2. The partition function used for acetylene neglects the isomerization to vinylidene. In other theoretical studies[47] of acetylene dissociation from 2000 to 3000 K, inclusion of this isomerization was important and served to increase the partition function by more than 10%. An increased partition function for acetylene will serve to decrease the computed rate constants in Figures 8−10 but again by a relatively small amount. With these kinds of corrections, the computed results of CCSD(T), MPW−SRP, and CAS+1+2+QC will likely drop into better contact with the experimental results in Tables 1 and 2 but may still be slightly higher than the measured values.

As discussed earlier, there are other experimental results that have not been part of the test of theory and experiment. Besides the measurements of the Sato group, additional measurements of H(D) + DCCD and low-pressure vinyl-radical dissociation measurements of Knyazev and Slagle[9] have not been included. We have decided not to pursue kinetics calculations for these processes because they involve more detailed considerations of the interaction between the buffer gas and the chemically activated vinyl radical. In a converse fashion, Knyazev and Slagle, who developed a considerable theoretical analysis, opted not to investigate isotopic reactions dominated by exchange reactions, such as D + HCCH. Consequently, an inclusive comparison of the entire experimental record will not be made at this time.

Although a comprehensive comparison will not be made here, we have extended the transition state electronic structure calculations of Knyazev and Slagle to the isotopic combinations necessary to consider D + HCCH in the fashion of Figures 8−10. (There is some ambiguity in regards to the imaginary frequency in this effort because the Knyazev and Slagle method uses an Eckart model for the potential that requires mapping out a reaction path in mass scaled reaction coordinates.) Instead of carrying out this mapping, we scaled the H + HCCH adjusted imaginary frequency by ratios determined from the CCSD(T) imaginary frequencies. The results are a modestly high representation of the H + HCCH results displayed in Figures 8−10,

an excellent representation of the measurements in Tables 1 and 2, and a substantial overestimation of all of the D + HCCH addition rate constants at lower temperatures. This behavior is unlike that of any of the eight methods examined here.

The reasons for this behavior reside in the use of a relatively low-level electronic structure method, UMP2, to characterize the structure and frequencies of the transition state. Relative to the eight methods here, the transition state for the UMP2 method is characterized by significantly higher frequencies, a noticeably more compact transition state structure, a very much higher barrier height (see Table 3), and a considerably higher imaginary frequency. The five lowest frequencies of the UMP2 method are always higher than the highest of the corresponding frequencies for any of the eight methods here. For these five lowest frequencies, the UMP2 values are typically higher by three standard deviations over the mean of the frequencies of the other methods. The C−H distance in the transition state is ∼0.2 Å shorter in the UMP2 calculation than that found in all of the other methods. At the lower temperatures, the zero-point energy corrected barrier and the tunneling (i.e., the imaginary frequency) dominate the rate, not the actual values of the frequencies. Because the barrier (and automatically the imaginary frequency) is optimized by Knyazev and Slagle to agree with lower temperature data of H + HCCH, any difficulties with the transition state frequencies are glossed over. However, at higher temperatures, the lower end of the transition-state frequency spectrum adds curvature to the rate constant that can be seen in Figures 8−10. This kind of curvature is missing in Knyazev and Slagle because the lower frequencies are too large, resulting in a fortuitously depressed rate constant. Furthermore, because the adjusted imaginary frequency of 771 cm^{-1} is in the middle of, and the adjusted zero-point energy corrected barrier of 4.04 kcal mol^{-1} is at the bottom of, the values in Table 3, the Knyazev and Slagle D + HCCH rate constants at low temperatures are too close to the H + HCCH rate constants, resulting in D + HCCH rates that are considerably higher than the error bars on the measured D + HCCH rates. The Knyazev and Slagle studies correctly identified the role of tunneling and the usefulness of the Eckart model but did not access sufficiently reliable electronic structure methods to represent a variety of isotopic combinations.

As all of the above discussion makes clear, the high temperature measurements of Tables 1 and 2 act to greatly extend the temperature range of experimental studies for the addition of hydrogen atoms to acetylene. This experimental temperature range places significant constraints on multiple components of a theoretical model. Because of the pressure insensitivity of the D + HCCH isotopic combination that is the focus of this study, these constraints go beyond the uncertainties of the buffer-gas/vinyl-radical interaction that controls the pressure dependence. The analysis suggests that the imaginary frequency, the barrier height, and details of the frequency change from reactant to transition state all contribute in varying degrees to secure agreement with experiment. Only the calculations most rooted in high level electronic structure methods can obtain agreement with experiment over the entire temperature range. Other popular methods, including G3 based methods and density functional methods, cannot obtain the same level of agreement over the entire temperature range.

Conclusions

In this work on the D + HCCH reaction, we have critically examined a large variety of electronic structure methods. To rationalize the present experimental results, high level electronic structure calculations have to be performed. With this high level of theory (CCSD(T)/aug-cc-pvtz shown in Table 7S), conventional TST calculations were performed for the high-pressure limiting rate constants. These calculations included modern estimates for quantum mechanical tunneling. The results can be expressed between 193 and 1600 K to within <±5% by the modified Arrhenius expression

$$k^{\mathrm{th}}_{1\mathrm{D}\infty} = 8.047 \times 10^{-15}\, T^{1.4083} \exp(-1518\ \mathrm{K/T})\ \mathrm{cm^3\ molecule^{-1}\ s^{-1}} \quad (11)$$

RRKM calculations were also carried out for the conditions of the present experiments. Pressure stabilization was found to be negligible in which case the rate constants can be expressed as $k_{\mathrm{bD}} = k_{1\mathrm{D}\infty}\langle k_{\mathrm{f}\epsilon}/(k_{\mathrm{f}\epsilon} + k_{\mathrm{b}\epsilon})\rangle = k_{\mathrm{bH}}$. The average fraction in brackets was likewise evaluated and found to be ∼0.6 over the present T range, giving theoretical estimates for k_{bD} that are 0.6 times eq 11. Conversely, the experimental high-pressure limit can be evaluated from eq 7 and compared to theory, eq 11. We find that the implied values from experiment are ∼29% lower than theory. We have also pointed out that inclusion of variational effects and anharmonic terms in the force field for acetylene both would decrease the theoretical value, eq 11, by as much as 10−15%, thereby making the discrepancy between theory and experiment almost within the error spreads of both the present and the lower-T experimental data. Then, application of the theory to the protonated case, H + HCCH, should give a reliable estimate for the high-pressure limiting rate constants, accurate to within 20−30%. To within <±9.5% accuracy, the theoretical estimate at the same level of theory between 193 and 1600 K is

$$k^{\mathrm{th}}_{1\infty} = 7.3673 \times 10^{-16}\, T^{1.7448} \exp(-1222\ \mathrm{K/T})\ \mathrm{cm^3\ molecule^{-1}\ s^{-1}} \quad (12)$$

Comparing eq 12 to the results of Payne and Stief[4] shows unambiguously that high-pressure limiting rate constants were not reached at the higher temperatures of their work. The subsequent conclusion, that the vinyl radical was a non-RRKM species,[5,8] is not correct. Knyazev and Slagle[9] correctly included tunneling and largely solved this paradox. However, these workers had to estimate $k^{\mathrm{th}}_{1\infty}$ by fitting the pressure dependent data on both H + HCCH and the vinyl-radical decomposition. They obtained a best value of

$$k^{\mathrm{th}}_{1\infty} = 6.05 \times 10^{-14}\, T^{1.09} \exp(-1328\ \mathrm{K/T})\ \mathrm{cm^3\ molecule^{-1}\ s^{-1}} \quad (13)$$

This latter value disagrees with eq 12 by ∼+50% at low-T and −40% at high-T. As discussed above, the Knyazev and Slagle[9] procedure required a double optimization of both $k^{\mathrm{th}}_{1\infty}$ and the energy transfer parameter. It is our suggestion that a new analysis of the pressure dependence is required starting with our less ambiguous assignment of $k^{\mathrm{th}}_{1\infty}$.

Acknowledgment. This work was supported by the U. S. Department of Energy, Office of Basic Energy Sciences, Division of Chemical Sciences, Geosciences, and Biosciences under Contract No.W-31-109-Eng-38.

Supporting Information Available: The calculated geometries, frequencies, and moments of inertia for acetylene, the transition-state, and the vinyl-radical, for all eight theoretical models, and for each of the three isotopic combinations, H +

HCCH, D + HCCH, and H + DCCH, are summarized in Tables 1S−8S. This material is available free of charge via the Internet at http://pubs.acs.org.

References and Notes

(1) Tollefson, E. L.; Le Roy, D. J. *J. Chem. Phys.* **1948**, *16*, 1057. Dingle, J. R.; Le Roy, D. J. *J. Chem. Phys.* **1950**, *18*, 1632.

(2) Volpi, G. G.; Zocchi, F. *J. Chem. Phys.* **1966**, *44*, 4010. Michael, J. V.; Weston, R. E., Jr. *J. Chem. Phys.* **1966**, *45*, 4632. Michael, J. V.; Niki, H. *J. Chem. Phys.* **1967**, *46*, 4969. Hoyermann, K.; Wagner, H. Gg.; Wolfrum, J.; Zellner, R. *Ber. Bunsen-Ges. Phys. Chem.* **1968**, *72*, 1004.

(3) Hoyermann, K.; Wagner, H. Gg.; Wolfrum, J.; Zellner, R. *Ber. Bunsen-Ges. Phys. Chem.* **1971**, *75*, 22.

(4) Payne, W. A.; Stief, L. J. *J. Chem. Phys.* **1976**, *64*, 1150.

(5) Keil, D. G.; Lynch, K. P.; Cowfer, J. A.; Michael, J. V. *Int. J. Chem. Kinet.* **1976**, *8*, 825.

(6) (a) Ishikawa, Y.; Sugawara, K.; Sato, S. *Bull. Chem. Soc. Jpn.* **1979**, *52*, 3503. (b) Kowari, K.; Sugawara, K.; Sato, S.; Nagase, S. *Bull. Chem. Soc. Jpn.* **1981**, *54*, 1222. (c) Sugawara, K.; Okazaki, K.; Sato, S. *Bull. Chem. Soc. Jpn.* **1981**, *54*, 2872.

(7) Ellul, R. Potzinger, P.; Reimann, R.; Camilleri, P. *Ber. Bunsen-Ges. Phys. Chem.* **1981**, *85*, 407.

(8) Harding, L. B.; Wagner, A. F.; Bowman, J. M.; Schatz, G. C.; Christoffel, K. *J. Phys. Chem.* **1982**, *86*, 4312.

(9) Knyazev, V. D.; Slagle, I. R. *J. Phys. Chem.* **1996**, *100*, 16899.

(10) Su, M.-C.; Michael, J. V. *Proc. Combust. Inst.* **2002**, *29*, 1219.

(11) Michael, J. V. *Prog. Energy Combust. Sci.* **1992**, *18*, 327.

(12) Michael, J. V. In *Advances in Chemical Kinetics and Dynamics*; Barker, J. R., Ed.; JAI: Greenwich, 1992; Vol. I, pp 47−112, for original references.

(13) Michael, J. V.; Sutherland, J. W. *Int. J. Chem. Kinet.* **1986**, *18*, 409.

(14) Michael, J. V. *J. Chem. Phys.* **1989**, *90*, 189.

(15) Michael, J. V.; Fisher J. R. In *Seventeenth International Symposium on Shock Waves and Shock Tubes*; Kim, Y. W., Ed.; AIP Conference Proceedings 208; American Institute of Physics: New York, 1990; pp. 210−215.

(16) Lim, K. P.; Michael, J. V. *Proc. Comb. Inst.* **1994**, *25*, 713 and references therein.

(17) Kumaran, S. S.; Su, M.-C.; Lim, K. P.; Michael, J. V. *Proc. Comb. Inst.* **1996**, *26*, 605.

(18) Michael, J. V.; Lifshitz, A. In *Handbook of Shock Waves*; Ben-Dor, G., Igra, O., Elperin, T., Lifshitz, A., Eds.; Academic Press: New York, 2001; Vol. 3, pp 77−105.

(19) Fisher, J. R.; Michael, J. V. *J. Phys. Chem.* **1990**, *94*, 2465.

(20) Holbrook, K. A.; Pilling, M. J.; Robertson, S. H. Unimolecular Reactions, 2nd Ed., John Wiley and Son, Ltd.: New York, 1996.

(21) Frisch, M. J.; Trucks, G. W.; Schlegel, H. B.; Scuseria, G. E.; Robb, M. A.; Cheeseman, J. R.; Zakrzewski, V. G.; Keith, T. A.; Montgomery, J. A., Jr.; Stratmann, R. E.; Burant, J. C.; Dapprich, S.; Millam, J. M.; Daniels, A. D.; Kudin, K. N.; Strain, M. C.; Farkas, O.; Tomasi, J.; Barone, V.; Cossi, M.; Cammi, R.; Mennucci, B.; Pomelli, C.; Adamo, C.; Clifford, S.; Ochterski, J.; Petersson, G. A.; Ayala, P. Y.; Cui, Q.; Morokuma, K.; Malick, D. K.; Rabuck, A. D.; Raghavachari, K.; Foresman, J. B.; Cioslowski, J.; Ortiz, J. V.; Stefanov, B. B.; Liu, G.; Liashenko, A.; Piskorz, P.; Komaromi, I.; Gomperts, R.; Martin, R. L.; Fox, D. J.; Al-Laham, M. A.; Peng, C. Y.; Nanayakkara, A.; Gonzalez, C.; Challacombe, M.; Gill, P. M. W.; Johnson, B. G.; Chen, W.; Wong, M. W.; Andres, J. L.; Head-Gordon, M.; Replogle, E. S.; Pople, J. A. *Gaussian 98*, Gaussian, Inc.: Pittsburgh, PA, 1998.

(22) Lynch, B. J.; Fast, P. L.; Harris, M.; Truhlar, D. G. *J. Chem. Phys. A* **2000**, *104*, 4811.

(23) Adamo, C.; Barone, V. *J. Chem. Phys*. **1998**, *108*, 664.

(24) Curtiss, L. A.; Raghavachari, K.; Redfern, P. C.; Rassolov, V.; Pople, J. A. *J. Chem. Phys*. **1998**, *109*, 7764.

(25) Baboul, A. G.; Curtiss, L. A.; Redfern, P. C.; Raghavachari, K. *J. Chem. Phys*. **1999**, *110*, 7650.

(26) MOLPRO is a package of ab initio programs written by Werner, H.-J.; Knowles, P. J. with contributions from Almlof, J.; Amos, R. D.; Berning, A.; Cooper, D. L.; Deegan, M. J. O.; Dobbyn, A. J.; Eckert, F.; Elbert, S. T.; Hampel, C.; Lindh, R.; Lloyd, A. W.; Meyer, W.; Nicklass, A.; Peterson, K.; Pitzer, R.; Stone, A. J.; Taylor, P. R.; Mura, M. E.; Pulay, P.; Schutz, M.; Stoll, H.; Thorsteinsson, T.

(27) Dunning, T. H., Jr. *J. Chem. Phys.* **1989**, *90*, 1007.

(28) Kendall, R. A.; Dunning, T. H., Jr.; Harrison, R. J. *J. Chem. Phys.* **1992**, *96*, 6796.

(29) Woon, D. E.; Dunning, T. H., Jr. *J. Chem. Phys.* **1993**, *98*, 1358.

(30) Knowles, P. J.; Hampel, C.; Werner, H.-J. *J. Chem. Phys.* **1993**, *99*, 5219.

(31) Werner, H.-J.; Knowles, P. J. *J. Chem. Phys*. **1985**, *82*, 5053.

(32) Knowles, P. J.; Werner, H.-J. *Chem. Phys. Lett*. **1985**, *115*, 259

(33) Werner, H.-J.; Knowles, P. J. *J. Chem. Phys*. **1988**, *89*, 5803

(34) Knowles, P. J.; Werner, H.-J. *Chem. Phys. Lett*. **1988**, *145*, 514.

(35) Langhoff, S. R.; Davidson, E. R. *Int. J. Quantum Chem*. **1974**, *8*, 61.

(36) Silver, D. W.; Davidson, E. R. *Chem. Phys. Lett*. **1978**, *52*, 403.

(37) Berkowitz, J.; Ellison, G. B.; Gutman, D. *J. Phys. Chem*. **1994**, *98*, 2744.

(38) Truhlar, D. G.; Isaacson, A. D.; Garrett, B. C. In *The Theory of Chemical Reaction Dynamics*; Baer, M., Ed.; CRC Press: Boca Raton, FL, 1985; Vol. 4, pp 65−137.

(39) Corchado, J. C.; Chuang, Y.-Y.; Fast, P. L.; Villa, J.; Hu, W.-P.; Liu, Y.-P.; Lynch, G. C.; Nguyen, K. A.; Jackels, C. F.; Melissas, V. S.; Lynch, B. J.; Rossi, I.; Coitino, E. L.; Fernanndez-Ramos, A.; Pu, J.; Albu, T. V.; Steckler, R.; Garrett, B. C.; Isaacson, A. D.; Truhlar, D. G. *POLYRATE* version 9.1; University of Minnesota: Minneapolis, MN, 2002.

(40) Coltrin, M. E.; Marcus, R. A. *J. Chem. Phys.* **1980**, *67*, 2609.

(41) Miller, W. H. *J. Am. Chem. Soc.* **1979**, *101*, 6810.

(42) Gilbert, R. G.; Luther, K.; Troe, J. *Ber. Bunsen-Ges. Phys. Chem.* **1983**, *87*, 169.

(43) Hippler, H.; Troe, J.; Wendelken, H. J. *J. Chem. Phys.* **1983**, *78*, 6709.

(44) Peterson, K. A.; Dunning, T. H., Jr. *J. Phys. Chem. A* **1997**, *101*, 6280.

(45) Scott, A. P.; Radom, L. *J. Phys. Chem.* **1996**, *100*, 16502.

(46) Lynch, B. J.; Truhlar, D. G. *J. Phys. Chem. A* **2001**, *105*, 2936.

(47) Kiefer, J. H.; Mudipalli, P. S.; Wagner, A. F.; Harding, L. B. *J. Chem. Phys.* **1996**, *105*, 8075.